Visualization of Anatomic Covariance Tensor Fields

Gordon L. Kindlmann[1] David M. Weinstein[1] Agatha D. Lee[2]
Arthur W. Toga[2] Paul M. Thompson[2]
[1]Scientific Computing and Imaging Institute, University of Utah, UT
[2]Laboratory of Neuro Imaging, Brain Mapping Division, Department of Neurology, UCLA School of Medicine, CA

Abstract—
The computation, visualization, and interpretation of brain variability remains a significant challenge in computational neuroanatomy. Current deformable registration methods can generate, for each vertex of a polygonal mesh modeling the cortical surface, a distribution of displacement vectors between the individual models and their average, which can be summarized as a covariance tensor. While analysis of anatomical covariance tensor fields promises insight into the structural components of aging and disease, basic understanding of the tensor field structure is hampered by the lack of effective methods to create informative and interactive visualizations. We describe a novel application of superquadric tensor glyphs to anatomic covariance tensor fields, supplemented by colormaps of important tensor attributes. The resulting visualizations support a more detailed characterization of population variability of brain structure than possible with previous methods, while also suggesting directions for subsequent quantitative analysis.

Keywords— **Visualization, Brain Modeling, Covariance Analysis, Software Tools, Computer Graphics Software**

I. Introduction

The quest to understand the anatomic variability of the human brain is important for three major applications in neuroscience. First, the functional organization of the brain differs widely across subjects, and measures are required to represent and visualize systematic patterns. A related application is to determine patterns of altered brain structure in diseases such as Alzheimer's, dementia, and schizophrenia, based on databases of brain scans. Finally, statistical information on anatomical variance is beneficial for computer visions algorithms that aim to identify and label specific brain structures automatically. Visualization is an essential component of understanding anatomic variability. Effective visualizations provide feedback for verifying the various algorithmic steps in computing variability, and offer flexible means of displaying and interacting with the data so as to form and refine hypothesizes about the structure and origins of anatomic variability.

This work represents anatomic variability as a field of covariance tensors over the cortical surface. In general, the challenge of tensor visualization is to convey the properties of individual tensor samples, as well as the large-scale spatial structure of changes in the tensor attributes, in such a way that does not overwhelm the viewer with an unintelligible mass of information. When visualizing covariance data computed from deformable registration of cortical surface models, we require the ability to inspect the degree and type of population variance at particular locations of interest on the cortical surface (such as the language areas of the brain in Alzheimer's disease), as well as the means of discerning overall patterns of variation that may represent novel indicators for biologically significant subpopulation characteristics.

This paper explores the combination of superquadric tensor glyphs and judicious application of colormaps to display individual tensors and the spatial structure of the tensor field, respectively. Glyphs, or icons, depict multiple data values by mapping them onto the shape, size, orientation, and surface appearance of a base geometric primitive [1]. Tensor glyphs generally indicate the tensor eigenvalues and eigenvectors by their scaling (shape) and orientation, respectively [2], as with the ellipsoidal glyphs commonly used to present diffusion tensor MRI data [3]. The limited previous work in visualizing anatomic covariance tensor fields employed nested semi-transparent ellipsoidal glyphs corresponding to a small set of confidence limits [4].

II. Methods

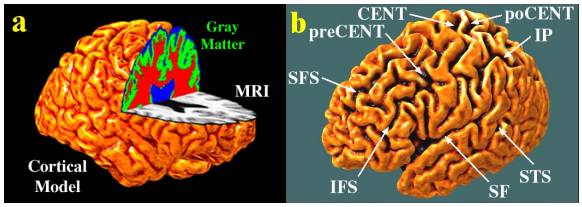

Fig. 1. Cortical surface models are extracted from MRI scans (a). On individual models, 3D parametric curves are manually traced to represent 72 sulcal landmarks (some shown in (b), defined in [7]), which in turn constrain the elastic deformation for cortical pattern matching.

The anatomic covariance tensors are generated from a non-linear pattern matching procedure presented in previous work [5], [6], [7]. MRI brain scans of 40 young healthy normal subjects were aligned with the ICBM-305 standardized brain with a 9-parameter affine transform, using established meth-

This work was supported by NIH National Center for Research Resources grants P41 RR12553, P20 HL68566, P41 RR13642, R21 RR19771, National Institute for Biomedical Imaging and Bioengineering grant EB 001561, and by NIMH/NIDA Human Brain Project grant P20 MH/DA52176 to the International Consortium for Brain Mapping.

ods [5], [7]. The aligned brains were then converted to 3D parametric models by smoothly deforming a high-resolution mesh to the MRI isosurface of the brain boundary, Fig 1(a). The major fissures in the brain surface, termed *sulci* and identified in Fig 1(b), have the same topology in all subjects. This enables *cortical pattern matching* to quantify the anatomic differences of interest as the minimum-energy 3D nonlinear elastic deformation that transforms the sulcal landmarks of an average model template onto those of each individual [7]. Anatomic variability is represented at each point on the average cortical mesh as the 3D covariance tensor of the displacement vectors induced by the deformations from the average to all individuals (after factoring out the affine components of the initial alignment).

A 3×3 covariance tensor $\mathbf{T}$ can be diagonalized as $\mathbf{T} = \mathbf{R}\mathbf{\Lambda}\mathbf{R}^{-1}$ where $\mathbf{\Lambda}$ is a diagonal matrix of eigenvalues and $\mathbf{R}$ is a rotation matrix that transforms the standard basis onto the eigenvector basis. Glyph-based tensor visualization transforms a base glyph geometry, G (typically a sphere), into a tensor glyph, $G_{\mathbf{T}}$ (typically an ellipsoid), by $G_{\mathbf{T}} = \mathbf{R}\mathbf{\Lambda}G$. Fig. 2(a) illustrates the space of tensor shapes with ellipsoidal glyphs, and shows how different tensor shapes can unfortunately present similar appearances. In contrast, superquadric glyphs reduce visual ambiguity and enhance the depiction of tensor structure.

We will now briefly summarize the superquadric glyph method presented in previous work [8]. Superquadric surfaces, shown in Fig. 2(b), are a continuum of shapes created by modifying the standard (θ, ϕ) parameterization of the sphere with two exponential parameters (α, β) [9]:

$$\mathbf{p}(\theta,\phi) = \begin{pmatrix} \cos^{\alpha}\theta \sin^{\beta}\phi \\ \sin^{\alpha}\theta \sin^{\beta}\phi \\ \cos^{\beta}\phi \end{pmatrix}, \quad \begin{matrix} 0 \le \theta \le 2\pi \\ 0 \le \phi \le \pi \end{matrix} \qquad (1)$$

where $x^{\alpha} = \mathrm{sgn}(x)|x|^{\alpha}$. The general strategy of superquadric tensor glyphs is that *edges indicate eigenvalue differences*. Mathematically, a difference in eigenvalues implies lack of rotational symmetry, which we visually emphasize by an edge on the glyph surface, which in turn more clearly indicates the orientation of the associated eigenvectors. When two eigenvalues are equal, the numerical indeterminacy of the associated eigenvectors is conveyed in the glyph with a circular cross-section. Fig. 2(c) demonstrates advantages of superquadrics over ellipsoids for depicting the range of tensor shapes.

The other component of our visualization method is the use of color scales, or colormaps, to indicate various attributes of the covariance tensors. This helps present large-scale patterns in the data. We also show the utility of conveying two tensor attributes simultaneously, by applying different maps on the mesh surface and on the tensor glyphs. Important attributes of the covariance tensor $\mathbf{T}$ include:

- $\|\mathbf{T}\|_F = \sqrt{\mathrm{tr}(\mathbf{T}\mathbf{T}^{\mathsf{T}})}$: The Frobenius norm
- FA($\mathbf{T}$): The *fractional anisotropy*, borrowed from the diffusion-tensor MRI literature [10]
- skew(λ_i): For eigenvalues $\lambda_1 \ge \lambda_2 \ge \lambda_3$, this varies between $-1/\sqrt{2}$ when $\lambda_1 \ge \lambda_2 = \lambda_3$ and $1/\sqrt{2}$ when $\lambda_1 = \lambda_2 \ge \lambda_3$, corresponding to linear (prolate) and planar (oblate) shapes, respectively.

In intuitive terms, $\|\mathbf{T}\|_F$ indicates the overall amount of variability, FA($\mathbf{T}$) indicates the extent to which the variability extends more in some directions than others (as opposed to being spherical or wholly rotationally symmetric), while skew(λ_i) indicates the type or shape of the anisotropy (the precise manner in which it differs from a sphere).

Additionally, the fraction of variability perpendicular to the cortical surface, which we term *surface-normal variance*, is an important aspect of the covariance tensor, as it indicates regional differences in brain shape that may be relevant for understanding degenerative disease, cortical dysplasias, or subtle abnormalities of cortical shape. We compute surface-normal variance as $\mathbf{n}^{\mathsf{T}}\mathbf{T}\mathbf{n}/\|\mathbf{T}\|_F$: the tensor contraction of covariance $\mathbf{T}$ along surface normal $\mathbf{n}$, normalized by Frobenius norm to vary between 0 and 1.

For visualization purposes, the field of covariance tensors was linearly downsampled by a factor of four, because individual glyphs must be large enough to see in the overall context of the cortical mesh, and because the covariance tensors do not change significantly within the span of a few mesh nodes. The glyphs were drawn slightly offset from the underlying mesh surface to better reveal the tensor attribute mapped onto the cortical surface.

We have developed the tensor visualization methods described here within BioPSE, a freely available integrated problem solving environment for the interactive investigation of large-scale scientific data [11]. The visualization algorithms have been implemented with modules in a reconfigurable dataflow network, thereby facilitating the exploration of different parameters and techniques.

III. Results

Fig. 3 demonstrates the difference between ellipsoid and superquadric glyphs on the medial side of the temporal lobe. Features that are better seen with the superquadrics include the concentration of planar shapes directly above the collateral sulcus, and the fact that glyphs with a planar orientation are generally tangential to the underlying surface.

Fig. 4 shows a combination of different attributes indicated on and beneath the field of superquadric glyphs. The most striking feature of the visualizations is that cortical areas with highest variability (as indicated by FA($\mathbf{T}$)) are those that developed most recently during human evolution, namely higher-order association areas and language cortex. Conversely, primary sensory and motor regions of the cortex are the least variable. The fractional anisotropy of variance is greatest in those brain re-

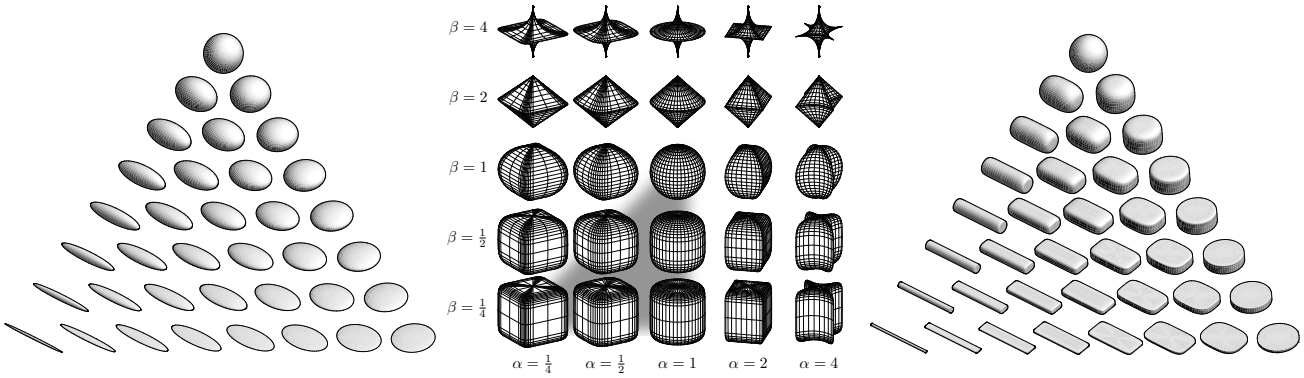

(a)Ellipsoid tensor glyphs (b)Space of superquadrics (c)Superquadric tensor glyphs

Fig. 2. Ellipsoidal glyphs (a) suffer from visual ambiguity. The range of superquadrics (b) used for tensor glyphs is highlighted with the gray triangle. Superquadric glyphs (c) differentiate shape and convey orientation more clearly than do ellipsoids.

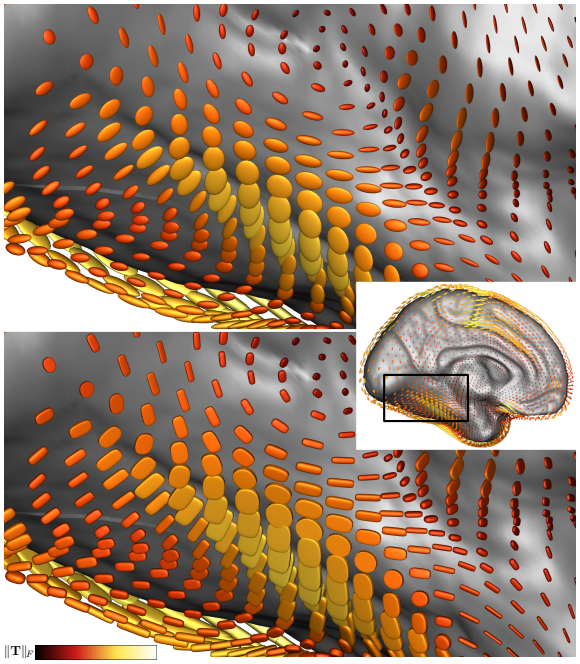

Fig. 3. Comparison of ellipsoid (top) and superquadric (bottom) glyphs, colormapped with $\|\mathbf{T}\|_F$.

gions that are asymmetrical (i.e. differ between left and right hemispheres), suggesting that strongly directional processes may occur during their formation.

The eigenvalue skew (b) differs markedly between temporal and parietal cortex on the lateral surface of the brain hemispheres, suggesting that most of the non-normal variance near the Sylvian fissure is relatively isotropic within the cortical sheet, but this variance becomes strongly concentrated along one direction in the parietal lobe, which is formed later in embryonic development. These principal directions of variance clearly vary by brain region, as expected from the different times of emergence of the fissures during fetal life. This cortical subdivision may help define the anatomical scope of genes that regulate brain fissuration. Sensorimotor regions are distinguished by their relatively low variance and their normal component of variance is relatively high [yellow colors, (c)], suggesting that these are the only structures whose tangential variability is well accommodated by a linear transformation to stereotaxic space.

IV. Discussion and Conclusion

The visualization method presented here is an important step in characterizing anatomic variability in the brain. Visualizing anatomic covariance tensors, both individually and as a group, illustrates the basic modes of anatomic variation and motivates new studies to better understand its origins. In light of the hypothesis that sulcus formation is a consequence of tension along white matter tracts [12], future work will seek to display and quantify the directional relationships between between anatomic variability and underlying diffusion tensor scans. The visualizations presented here are geared towards exploration of the tensor values themselves, but additional visualizations can extract or quantify higher-order tensor field structure, for example hyperstreamlines [13] or topological analysis [14].

References

[1] F. Post, F. Post, T. van Walsum, and D. Silver, "Iconic techniques for feature visualization," in *Proc. IEEE Visualization 95*, pp. 288–295, 1995.

[2] R. Haber and D. McNabb, *Visualization Idioms: A Conceptual Model for Scientific Visualization Systems*, pp. 74–93. IEEE, 1990.

[3] P. Basser, J. Mattiello, and D. L. Bihan, "MR diffusion tensor spectroscopy and imaging," *Biophysics Journal*, vol. 66, no. 1, pp. 259–267, 1994.

[4] P. Thompson and A. Toga, "Detection, visualization and animation of abnormal anatomic structure with a deformable probabilistic brain atlas based on random vector field transformations," *Medical Image Analysis*, vol. 1, no. 4, pp. 271–294, 1997.

[5] J. Mazziotta, A. Toga, and A. E. *et al.*, "A probabilistic atlas and reference system for the human brain," *Journal of the Royal Society*, vol. 356, pp. 1293–1322, Aug. 2001.

[6] P. Thompson, M. Mega, C. Vidal, J. Rapoport, and A. Toga, "Detecting disease-specific patterns of brain structure using cortical pattern matching and a population-based probabilistic brain atlas," in *Proc. 17th International Conference on Information Processing in Medical Imaging (IPMI2001)*, pp. 488–501, June 2001.

[7] P. Thompson, K. Hayashi, G. de Zubicaray, A. Janke, S. Rose, J. Semple, D. Herman, M. Hong, S. Dittmer,

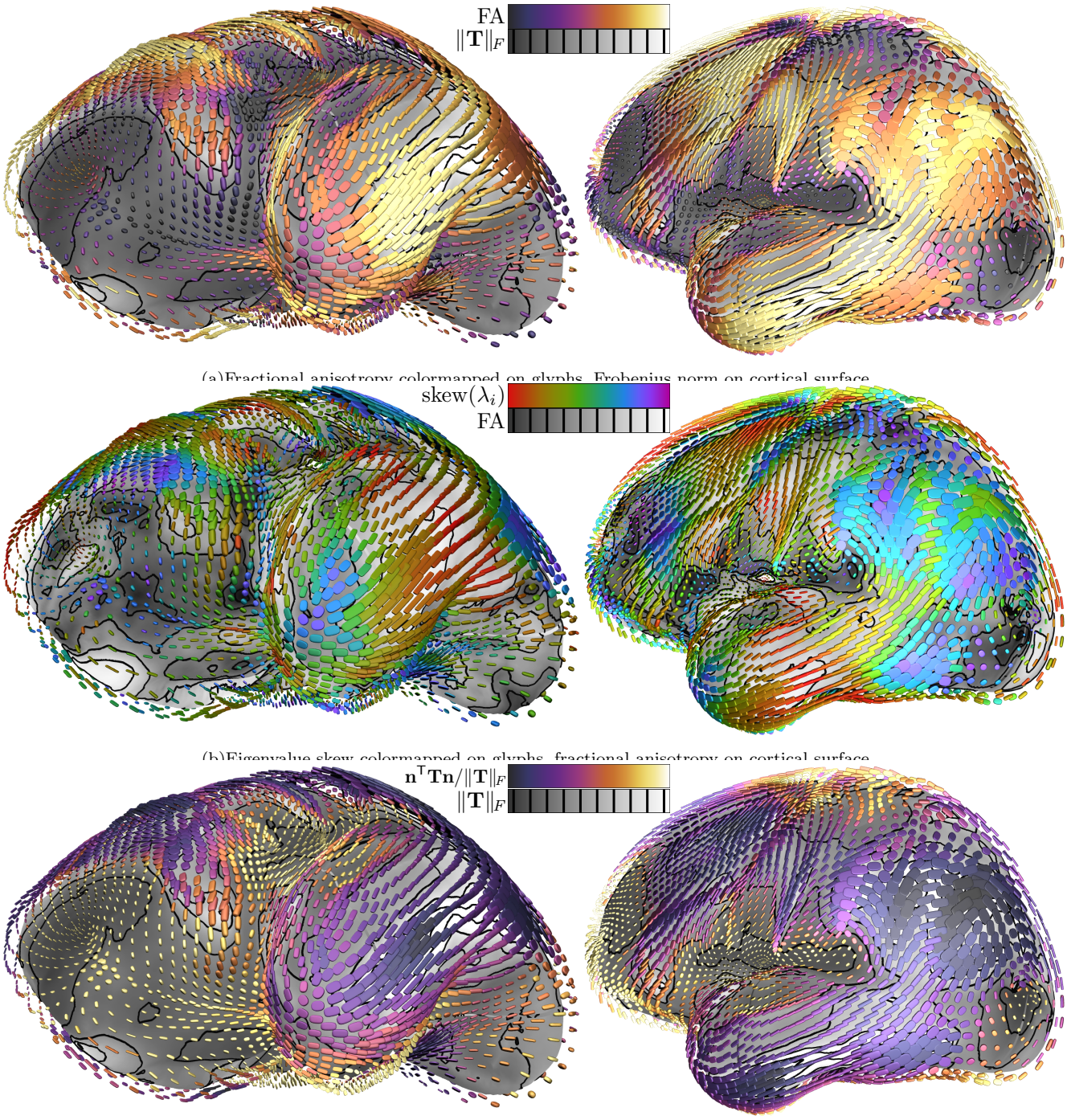

(a)Fractional anisotropy colormapped on glyphs, Frobenius norm on cortical surface

(b)Eigenvalue skew colormapped on glyphs, fractional anisotropy on cortical surface

(c)Surface-normal variance colormapped on glyphs, Frobenius norm on cortical surface

Fig. 4. Sequence of quantities colormapped on superquadric glyphs, with gray-scale indication on the underlying mesh surface.

D. Doddrell, and A. Toga, "Dynamics of gray matter loss in Alzheimer's disease," *Journal of Neuroscience*, vol. 23, pp. 994–1005, Feb. 2003.

[8] G. Kindlmann, "Superquadric tensor glyphs," in *Proc. IEEE TVCG/EG Symposium on Visualization 2004*, pp. 147–154, May 2004.

[9] A. Barr, "Superquadrics and angle-preserving transformations," *IEEE CG & A*, vol. 18, no. 1, pp. 11–23, 1981.

[10] P. Basser and C. Pierpaoli, "Microstructural and physiological features of tissues elucidated by quantitative-diffusion-tensor MRI," *Journal of Magnetic Resonance, Series B*, vol. 111, pp. 209–219, 1996.

[11] BioPSE: Problem Solving Environment for modeling, simulation, and visualization of bioelectric fields. Scientific Computing and Imaging Institute (SCI), http://software.sci.utah.edu/biopse.html, 2002.

[12] D. V. Essen, "A tension-based theory of morphogenesis and compact wiring in the central nervous system," *Nature*, vol. 385, pp. 313–318, Jan. 1997.

[13] T. Delmarcelle and L. Hesselink, "Visualizing second-order tensor fields with hyper streamlines," *IEEE CG & A*, vol. 13, no. 4, pp. 25–33, 1993.

[14] L. Hesselink, Y. Levy, and Y. Lavin, "The topology of symmetric, second-order 3D tensor fields," *IEEE TVCG*, vol. 3, Jan–Mar 1997.